Scientific and Technological Alliance for Guaranteeing the European Excellence in Concentrating Solar Thermal Energy

Project Deliverable 7.6:

Assessment of thermal energy storage options to direct steam generation power plants

WP7 – Task 7.3.1	Deliverable 7.6
Due date:	January/2017
Submitted	January/2017
Partner responsible	Fraunhofer ISE
Person responsible	Thomas Fluri (F-ISE)
Author(s):	Rocío Bayón (CIEMAT), Esther Rojas (CIEMAT), Bernhard Seubert (F-ISE), Martin Karl (F-ISE), Verena Zipf (F-ISE), Anton Neuhäuser (F-ISE)
Document version:	1
Reviewed/supervised by:	
Dissemination Level	PU

Table of contents

Figures

Tables

1. Introduction

Up to now, latent heat energy storage has been achieved with phase change materials (PCMs) undergoing solid to liquid transitions, which means that heat transfer efficiency, is limited by the thermal conductivity of the solid phase. This implies that a constant power in discharge cannot be attained due to the variable thermal resistance imposed by the solid phase formation. On the other hand, storage capacity with the current latent heat storage designs imposes the size of the heat exchanger, since storage system and heat exchanger become the same equipment.

In order to overcome these drawbacks, the most innovative strategies aim to uncouple heat transfer from storage capacity, which means that, somehow, the storage material has to move. These strategies can be addressed from either the heat exchanger equipment design point of view or the PCM point of view. The first one has been FISE's approach and the second one has been CIEMAT's approach.

2. Fraunhofer ISE Contribution

The contribution of Fraunhofer ISE consists of two subsections. First, an experimental setup with lab prototypes of a screw heat exchanger and, second, a simulation study based on the developed screw heat exchanger in a solar thermal power plant with latent heat storage.

2.1. Experimental Setup of Fraunhofer's Screw Heat Exchanger Prototype

The aim was to proof the concept of an active latent thermal storage concept based on screw heat exchangers (SHE). Therefore, two prototypes have been built. The first prototype was based on thermal oil as a heat transfer fluid (HTF) in order to reduce complexity and to have only a phase change on the salt side. Additionally the achievable measurement accuracy is higher with thermal oil. The second prototype was operated with water/steam as HTF.

2.1.1. System Layout and Experimental Setup

In the following figure, the system layout of the experimental setup of the screw heat exchanger (SHE) and the relevant measurement points are shown:
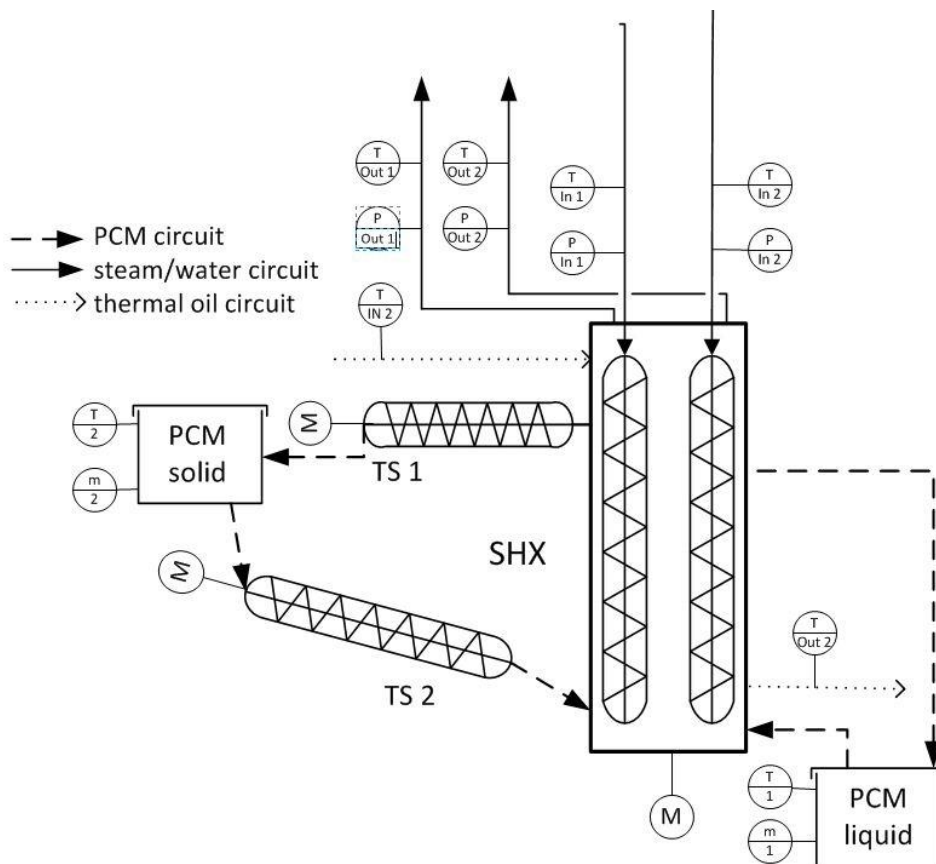
Figure 1. System layout of the experimental setup for the testing of the screw heat exchanger (SHE) with steam/water with all relevant measurement points: T = temperature, P = pressure, m = mass.

The developed test rig used for the experimental characterization of the heat transfer in the SHE is shown in Figure 2. For charging the storage, the PCM, an eutectic mixture of sodium nitrate ($NaNO_3$) and potassium nitrate (KNO_3) with a melting temperature of $T_{PCM,pc} = 221$ °C, is transported with transport screw 2 from the granules storage tank to the SHE. Inside the SHE the PCM melts when the thermal oil (in the first series of tests) or in further experiments steam is flowing through the hollow shaft, the hollow flights and the hollow trough. The phase change material (PCM) is stored in liquid state in a second storage tank below the SHE. For discharging, the liquid PCM storage tank is lifted above the SHE so that liquid PCM enters the SHE and crystallizes on the heat exchanger surface. Due to a self-cleaning effect inside the SHE, the crystallized PCM is wiped off the surface and crushed to pieces. By the turning screws, the PCM granules are transported to the outlet of the SHE, pass the transport screw 1 and are stored in the granules storage tank [2].

Figure 2. Experimental setup of the active latent heat storage with a screw heat exchanger (SHE): in the picture, the SHE and the PCM-circuit are shown [4]

The screw heat exchanger comprises two parallel hollow screw shafts with hollow flights (see Figure 4). One screw is single threaded, the other is double threaded (see Figure 3). Due to this arrangement the ability of self-cleaning of the SHE is fostered.
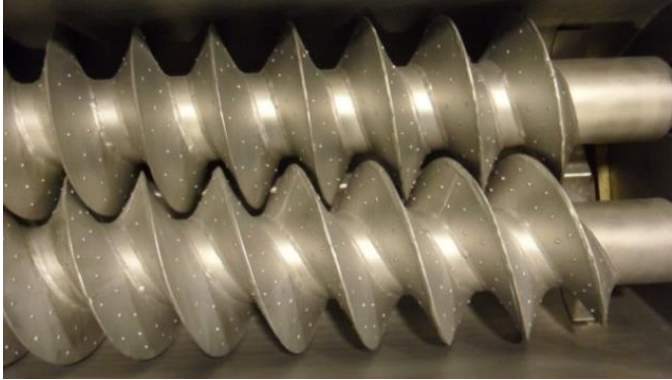
Figure 3: Screw shafts of the heat exchange [4]
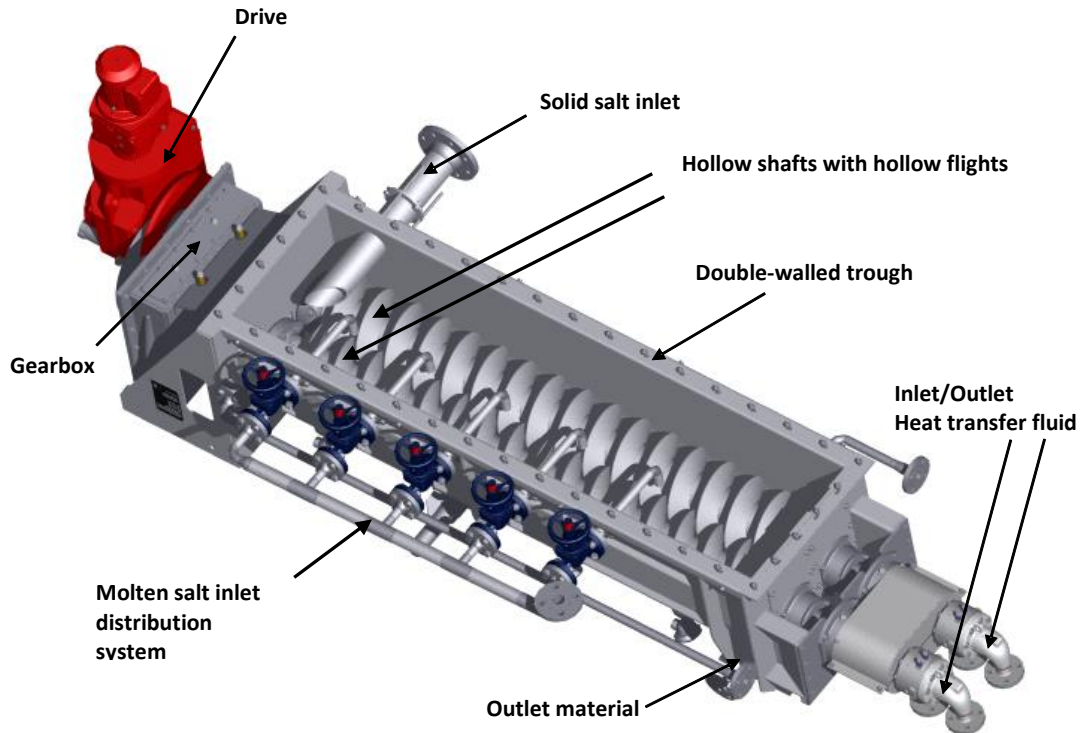
Figure 4. Screw heat exchanger, which is used in the latent storage to actively transport the phase change material during charging (melting) and discharging (crystallization)

2.1.2. Development of the Salt Distribution for the Liquid and Solid Phase

Figure 5. Different salt distribution systems in the prototype. Left: original system from supplier, middle: first improved prototype; right: optimized system

Liquid Salt Distribution: The manufacturer of the SHX delivered a salt distribution system to distribute the molten salt on the screw flights (see Figure 5, left). During the first tests the distribution system showed a poor performance: only 30% of the screw flight was covered with molten salt. In order to improve the usage of the screw flight ideas for new distribution principles were developed in the team. The most promising idea was a channel that is flooded with molten salt and overflowing the walls (see middle). A first prototype showed a strong

9

dependency on the accuracy of the horizontal orientation. It was decided to build a new version with a wall that distributes the salt through small holes. This allows for a raised fluid level above the holes that can leverage inaccuracy in horizontal orientation (see Figure 5, right). Additionally a trace heating was applied in order to prevent the salt from freezing in the holes and on the vanes of the distribution system. This approach could improve the usage of the screw flight area up to approx. 70 %.

Figure 6. Inlet system for liquid PCM into the SHE

Solid Salt Distribution: During the first tests we learned that the screws transport the solid material not directly in axial direction but also with a radial component. Therefore looking in the transport direction (see Figure 5, middle) the material was transported from the middle between the screws where it originally entered the heat exchanger to the right wall. In order to improve the distribution in the screw the tube of the inlet screw was cut in order to introduce the solid salt on the left front corner of the trough. This improved the distribution but still solid material was transported to the outlet of the heat exchanger. Therefore the outlet was blocked by a sheet of metal and the rotation of the screws was reversed in intervals in order to prevent the salt form blocking the screws at the barrier.

2.1.3.   Scraped Surface Heat Exchanger

Within the screw heat exchanger test rig it is not possible to determine the heat transfer coefficient of the crystallization process of the PCM precisely. This is due to the emerging PCM-layer and the wetting of the surface, which are not determinable exactly. Nevertheless, in order to determine the heat transfer coefficient, a less complex model was built, which is depicted in Figure 7 and described in more detailed in [4]. A scraped surface heat exchanger was used. The cylindrical container, which contains the PCM, is being cooled by thermal oil from the outside. The PCM is mixed by an agitator which also abrades the crystallizing PCM

from the surface. Due to the geometry of the agitator and the container, a layer of PCM of a certain thickness is formed and hence, the heat transfer coefficient can be determined.

Thermal oil thermostat

Agitator

Cylindrical container

Controller thermostat

Measurement data logging
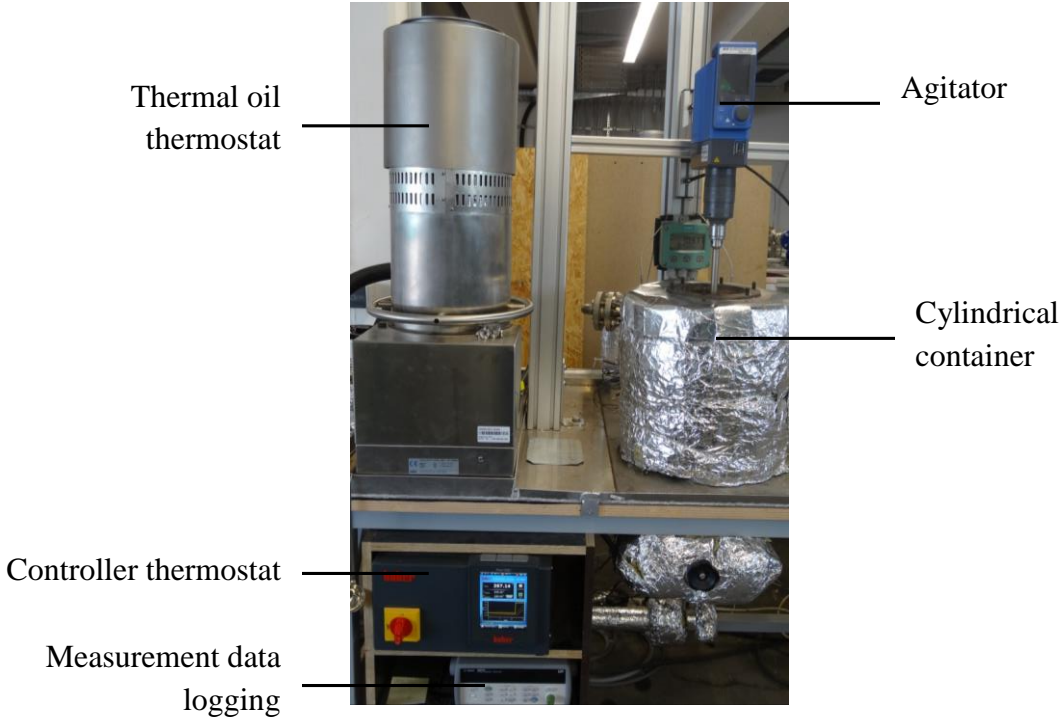
Figure 7: Test rig with scraped surface heat exchanger in order to ascertain the heat transfer coefficient of the phase change material during crystallization [4]

2.2. Experimental Results, Calculation of Heat Transfer Coefficient and Further Reaching Concepts

2.2.1. Test Runs with Oil as HTF

Measurement data for one complete cycle is shown in Figure 8. First at about 11:30 molten salt is solidified. The heat released during this process is not exceeding the heat losses therefor the transferred heat is negative but less than during the melting process that starts about 16:30.

Heat and Massflow
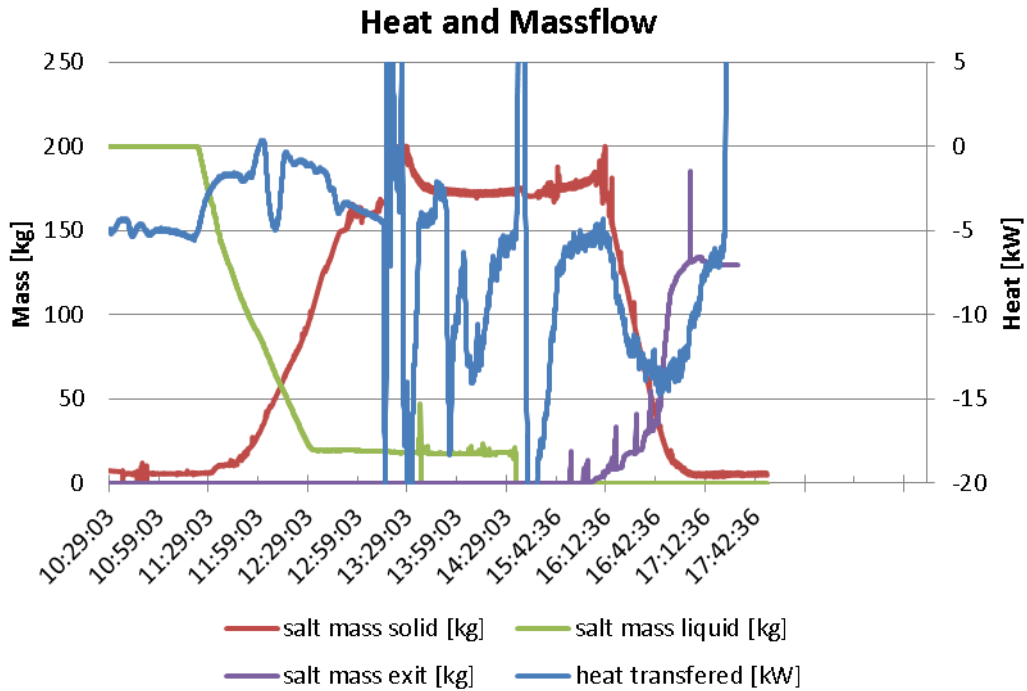
Figure 8. Measured data for one test cycle with Oil as HTF (discharging and charging)

2.2.2. Test Runs with Water/Steam as HTF

Charging of the storage: The goal of the first experiments with water/steam as HTF was proving the ability of melting the PCM while the incoming steam condenses inside the shafts. Due to the melting temperature of the salt (221 °C) and the needed ΔT, steam parameters were at the facilities maximum 227°C / 26.5 bar. The inlet temperature of the thermal oil that is streaming through the trough of the heat exchanger has 227° as well. The inlet temperature of the salt granulate is at 180 °C.

For heating up the system, steam/water valves before and after the SHX were slightly open so that steam streams through the SHX without any significant condensation. By increasing the thermal oil temperature of the tube/shell evaporator, steam parameters inside the SHX rose. In parallel hot salt granulate was transported into the SHX's trough. Upon the incoming steam reaching the melting point of the storage media, the media melted in contact with the outer surface of the hollow shafts. Short before the steam had its set point temperature the valves at the backflow steam line were closed and SHX was controlled condensate side. Steam was condensing during melting the salt granulate. The sight glass in the backflow showed water in front of the condensate trap while the molten salt was dripping from the outlets of the SHX.
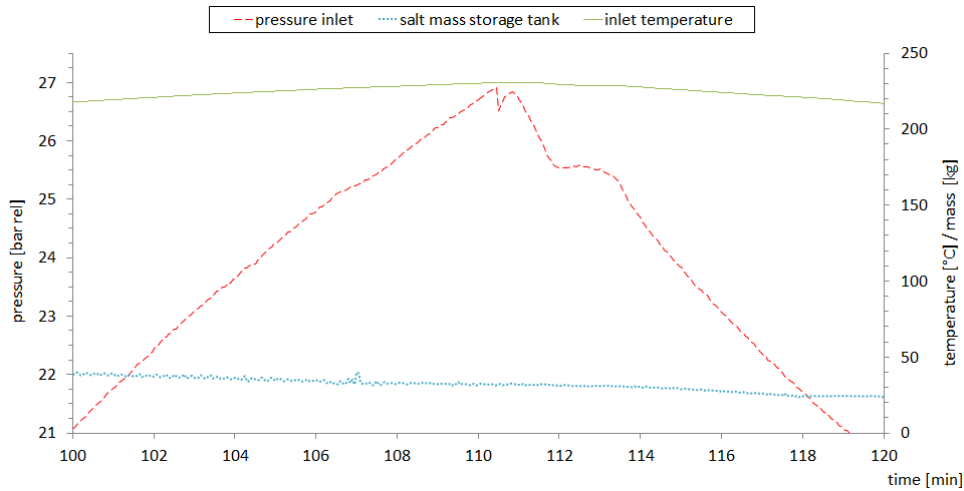
Figure 9. Steam parameters inside the SHX, decreasing salt mass inside the storage tank

Discharging of the storage: To assess the discharging behavior of the SHX, pressurized water (180°C / 10 bar) should be vaporized by passing the channels of the hollow shaft. In parallel the outer surface of the shafts are constantly covered by molten salt (231°C), which crystallized on the surface. The water should be vaporized by the latent heat of the crystallizing salt. In a first approach, the lowest possible mass flow of pressurized water was passing the salt heated SHX in order to vaporize. The sight glass in the backflow of the SHX showed streaming water without steam bubbles. The water flow was at its lowest and the heat input from the molten salt could not be further increased.

Starting points for realizing the direct steam production inside the SHX can be condensate recirculation, further improvement of the insulation and a controlled needle valve in the backflow of the SHX for finer adjustments of the water flow. In order to discharge the storage at reasonable steam parameters a batch process was performed (compare Figure 10). Inlet and outlet of the water-filled shafts were closed. The incoming heat from the crystallizing salt pressurized the closed hollow shafts. At a pressure around 13 bar the valve at the backflow was shortly opened in order to produce steam during the expansion of the trapped fluid. The sight glass showed streaming steam.
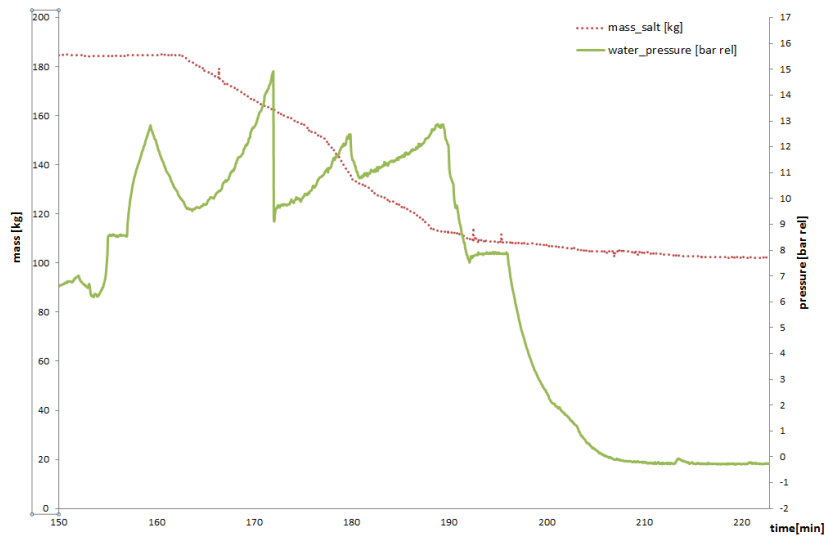
Figure 10. Water pressure inside the SHX, decreasing salt mass inside the storage tank

2.2.3. Examination of Heat Transfer Characteristics of the Screw Heat Exchanger

In order to determine the overall heat transfer coefficients in the SHE during melting $U_{SHE,m}$ and crystallization $U_{SHE,c}$ the thermal power transferred to the oil $\dot{Q}_{Oil}$ was measured. The results of these measurements are shown in Figure 11. Before conducting each experiment the heat losses $\dot{Q}_{loss}$ were determined. With this value the actual transferred thermal power can be calculated as well as the overall heat transfer coefficient by considering the transfer area of the SHE (A_{SHE} = 4.6 m², whereby 1.6 m² per screw and 1.4 m² trough) and the logarithmic temperature difference of the oil.
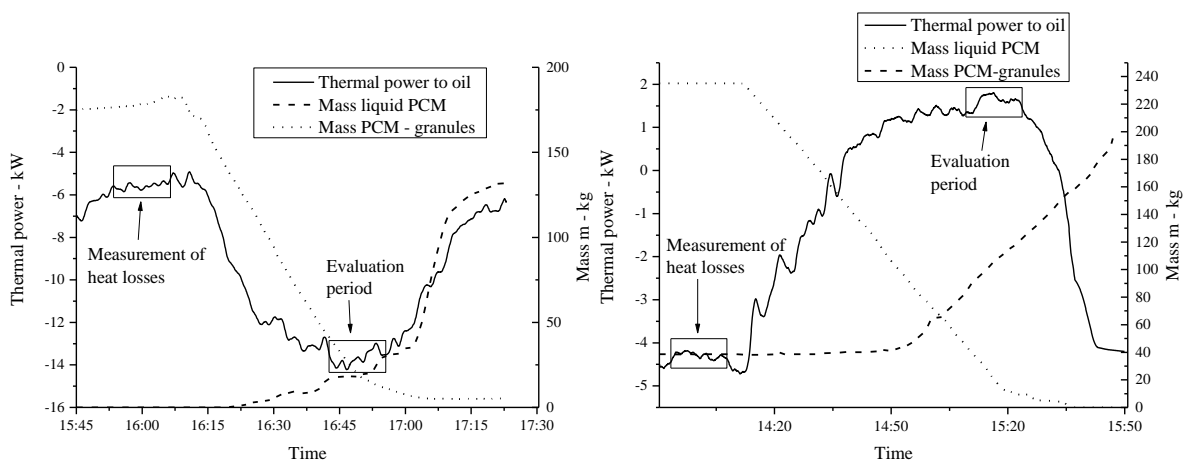
Figure 11. Melting (left) and crystallization (right) of the phase change material in the screw heat exchanger. Course of thermal power in thermal oil Q_{oil} and the PCM – mass in solid and liquid storage tank.

The results of the melting experiments are shown in Table 1, assuming that the heat transfer area A_{SHE} was wetted only about 73 %.

Table 1. Experimental conditions and results for melting of PCM in the SHE

Speed of rotation SHE shaft 1	Temperature PCM in	Volumetric flow oil	Temperature difference PCM/oil	Transferred thermal power	Uncertainty thermal power	Overall heat transfer coefficient	Uncertainty $U_{SHE,m}$
n_{sh} - 1/min	$T_{PCM,in}$ - °C	$\dot{V}_{oil}$ - m³/h	$\Delta T_{PCM\text{-}oil}$ - K	$\dot{Q}_{tr}$ - kW$_{th}$		$U_{SHE,m}$ - W/m²K	
1.4	195	10.2	9.0	-9.3	±8.6%	**310**	±12.9%
1.4	194	10.0	8.0	-8.3	±9.6%	**308**	±13.9%

The results of the crystallization experiments are shown in Table 2, assuming that the heat transfer area A_{SHE} was wetted only about 60 %. $U_{SHE,c}$ is much smaller compared to $U_{SHE,m}$ due to the layer of solid PCM, which emerges on the heat transfer surface of the SHE during crystallization in between times when the heat transfer surface is wiped clean due to the self-cleaning effect. This layer acts as an additional thermal resistance.

Table 2. Experimental conditions and results for the crystallization of PCM in the SHE

Speed of rotation SHE shaft 1	Temperature PCM in	Volumetric flow oil	Temperature difference PCM/oil	Transferred thermal power	Uncertainty thermal power	Overall heat transfer coefficient	Uncertainty $U_{SHE,c}$
n_{sh} - 1/min	$T_{PCM,in}$ - °C	$\dot{V}_{oil}$ - m³/h	$\Delta T_{PCM\text{-}oil}$ - K	$\dot{Q}_{tr}$ - kW$_{th}$		$U_{SHE,c}$ - W/m²K	
0.7	240	11.2	10.0	5.5	±11.2%	**197**	±11.9%
0.7	229	11.1	9.7	6.1	±10.1%	**225**	±11.4%

2.2.4. Calculated Overall Heat Transfer Coefficients U for a Scaled-up SHE with Steam as Heat Transfer Fluid

An optimized geometry for an enlarged SHE which uses steam as heat transfer fluid was determined. Therefore, material and manufacturing cost have been investigated, and geometrical parameters have been changed iteratively and the resulting cost per kilowatt have been calculated. By that means, a geometry for a SHE with minimal cost per kilowatt has been determined by an optimization. It has four parallel shafts and a thermal power of 1.2 MW for charging and 0.84 MW for discharging (both for $\Delta T_{PCM\text{-}steam} = 10K$). The overall heat transfer coefficients for an enlarged SHE were calculated. The values for the heat transfer coefficients of the PCM are conservative values based on the values calculated from the measurements. The resulting overall heat transfer coefficients are $U_{SHE,m} = 320$ W/m²K for charging and $U_{SHE,c} = 243$ W/m²K for discharging. Further reaching information can be found in [3].

2.2.5. Concept for a High Pressure Steam Screw Heat Exchanger

In order to operate the SHE with a pressure of 100 bar, FEM simulations have shown that an unacceptable wall thickness of the flights would be needed [1]. In order to avoid this, a heat

pipe concept has been developed, which uses an organic working fluid inside the flights (see Figure 12). When the storage is charged, high pressure steam condenses in the center of the shaft. The energy is transferred with the internal heat exchanger onto the organic fluid which evaporates and condenses again on the inner flight surface. Hence, the PCM on the outside melts. With a wick or by grooves the organic fluid is being transported back to the shaft center, which has to be investigated in further researches. A more detailed description of the concept can be found in [4].
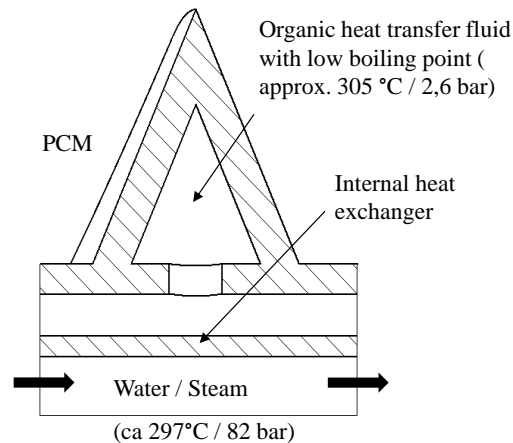
Figure 12. Concept for high steam pressure with an organic heat transfer fluid inside the flight of the screw heat exchanger

2.3. Simulation Study with Investigated Latent Heat Storage in a 50 MW$_{el}$ CSP Plant

The application of the screw heat exchanger in a solar thermal power plant with a nominal capacity of 50 MW$_{el}$ was examined. The aim was to assess the use of the SHE in such a system on an economical approach. With the generated measurement data of the test rig the developed simulation model could be validated. A detailed description of the simulation models and the components can be found in [2,4,5].

Two different heat storage layouts in a 50 MW DSG solar thermal power plant with linear Fresnel collectors are discussed in this work. Both layouts combine the mode of latent and sensible heat storage. The screw heat exchanger (SHE) described above allows for phase change during heat transfer. By mechanically transporting the PCM it increases the heat transfer in the heat exchanger compared to passive PCM concepts, such as finned tube concepts. As a reference, a system without storage has been examined as well.

The system layouts which were assessed are based on a 50 MW DSG plant with:

    a. A two tank storage with gas burner (compare Figure 13)
    b. A solar only three tank storage system (compare Figure 15)
    c. A system without storage

The gas burner in plant a) is needed in order to superheat the steam during storage discharge

to the turbine inlet temperature $T_{in} = 540$ °C. In plant b) the burner is not needed, as the superheating takes place in the heat exchangers.
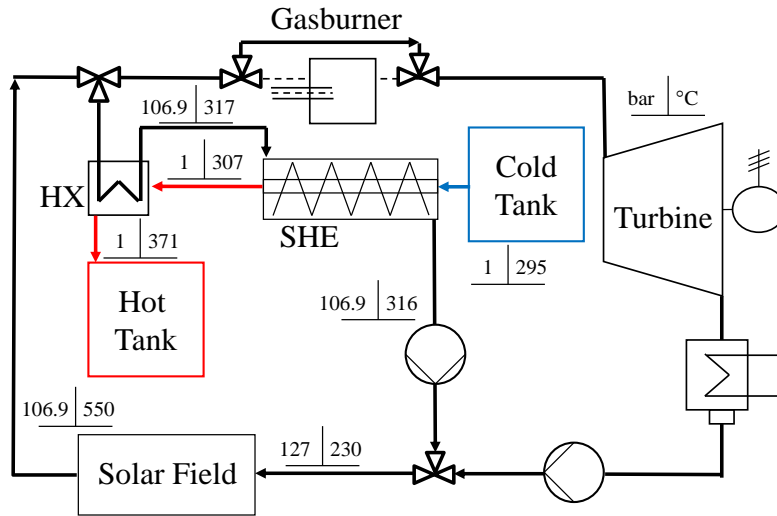
Figure 13: System layout of a) a 50 MW direct steam generating (DSG) plant with a two tank storage and auxiliary gas burner in daytime operation
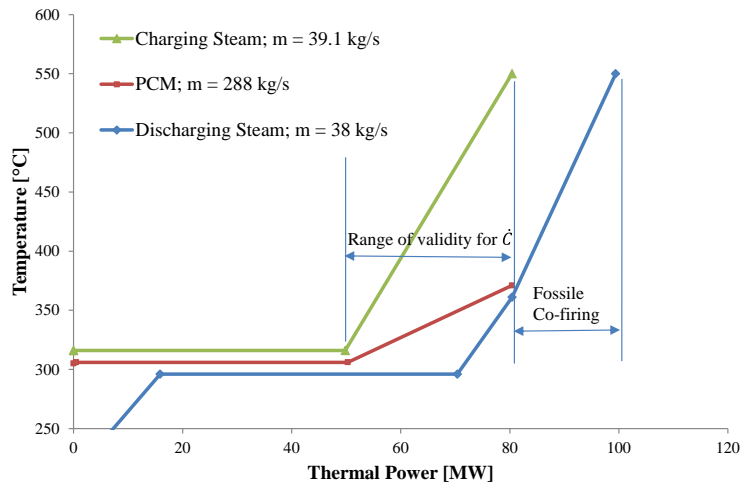
Figure 14: T-Q-diagram showing the charge and discharge of a combination of latent and sensible heat storage in a 50 MW DSG solar thermal power plant for a) a two tank configuration with additional fossil heater during discharge [5]
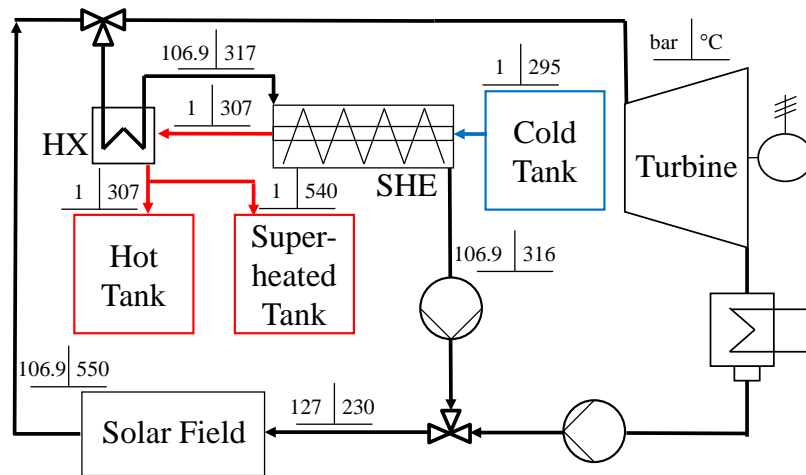
Figure 15. System layout of b) a 50 MW DSG plant with a three tank storage in daytime operation
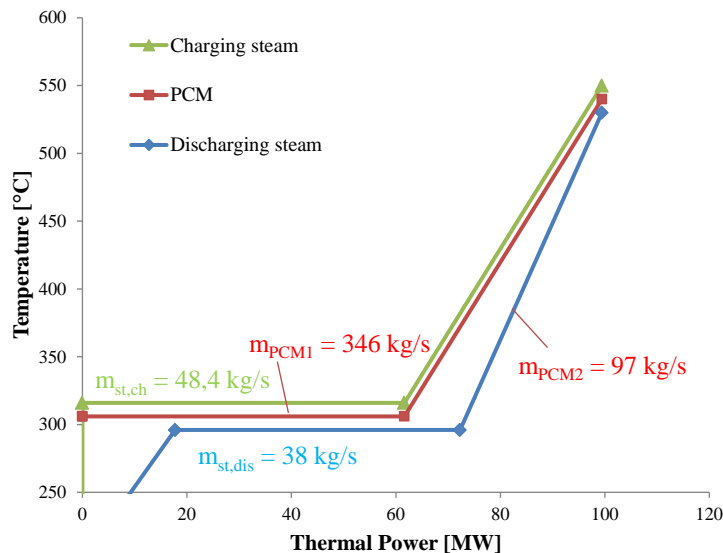
Figure 16: T-Q-diagram showing the charge and discharge of a combination of a latent and a sensible heat storage in a 50 MWel DSG solar thermal power plant for b) a three tank configuration [5]

The annual energy yield of the power plants was calculated. Different parameters, such as the solar field size, the storage capacity or the heat transfer in the heat exchanger were varied in discrete steps. From the annual energy yield and cost assumptions for all system components, the levelized cost of electricity (LCOE) were calculated for each simulation run, in order to compare different systems and to find an optimal design.

For a) the minimal LCOE are 0.143 €/kWh, for b) 0.134 €/kWh and for c) 0.129 €/kWh. As storages can add to the market value of electricity, an increase in LCOE for the systems with storage is acceptable. The difference of LCOE of a) and b) is in the range of possible uncertainties in the cost assumptions. This gap could be more distinct if more factors are taken into account and optimized, as e.g. the heat exchanger area. Clearly, the LCOE can be further decreased if the heat exchanger area is adapted to the storage capacity and not to the

discharging power needed. An optimum considering this effect still has to be calculated. A sensitivity study showed that the solar field costs have a high influence on the LCOE. By decreasing the storage cost by 20 %, the LCOE can be decreased by 5 %. To do so, the screw heat exchanger should be further optimized. A first geometric design optimization has already been conducted. To decrease the storage cost further, the thermal efficiency of the screw heat exchanger should be increased (e.g. by optimization of the process parameters). Another option to decrease the storage cost is to optimize the temperature difference between the charging / discharging water and the PCM. These points should be further investigated in future simulations studies. In general, the results show that the storage technology developed has a good potential to compete with existing thermal storage technologies.
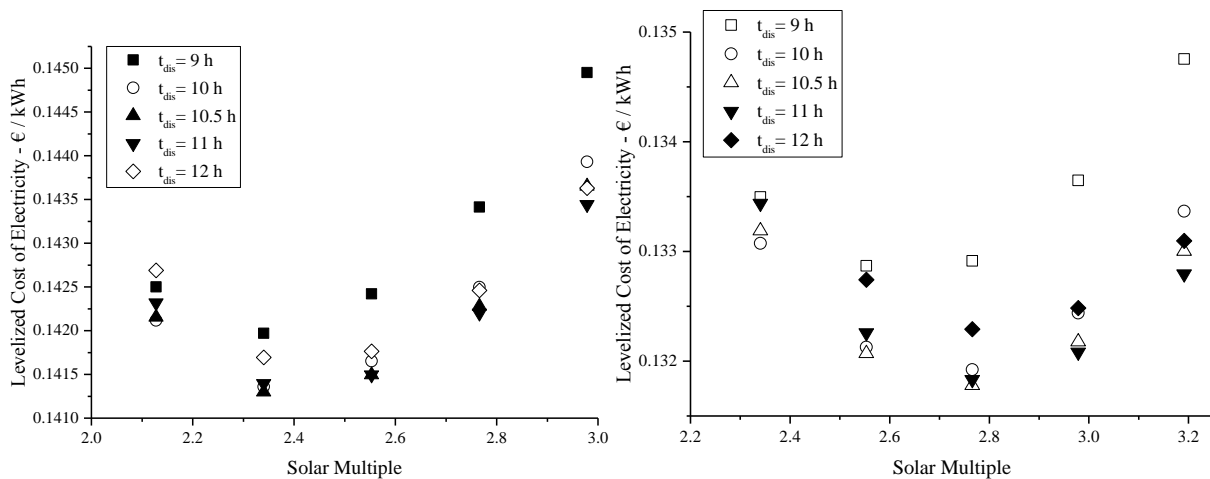
Figure 17. LCOE of a 50 MW direct steam generating (DSG) power plant with a) two-tank-storage and auxiliary fossil gas burner (left) or b) three-tank-storage without auxiliary fossil gas burner for a variation of the solar multiple (SM) and the possible storage discharge time t_{dis}

Sensitivity analysis: The cost can vary depending on market and local conditions. In order to see the impact of these fluctuations on the LCOE, the cost assumptions have been varied in a range of +/- 20% in a sensitivity analysis. The resulting LCOE for this variation of several factors have been calculated (see Figure 18). The interest rate has the highest influence on the LCOE, followed by the solar field cost. Regarding the storage, the LCOE can be changed by 5 % by reducing the storage costs by 20 %. It can be concluded, that the first priority should be laid on improving the solar field layout, as this has the best lever on the LCOE. But also the reduction of storage cost can decrease the LCOE by as much as 5 %. Looking at the cost assumptions, the potential in decreasing the storage cost for the new storage concept can mainly be seen in decreasing the cost for the screw heat exchanger, as about 50 % of total storage costs are attributed for the screw heat exchangers [5].
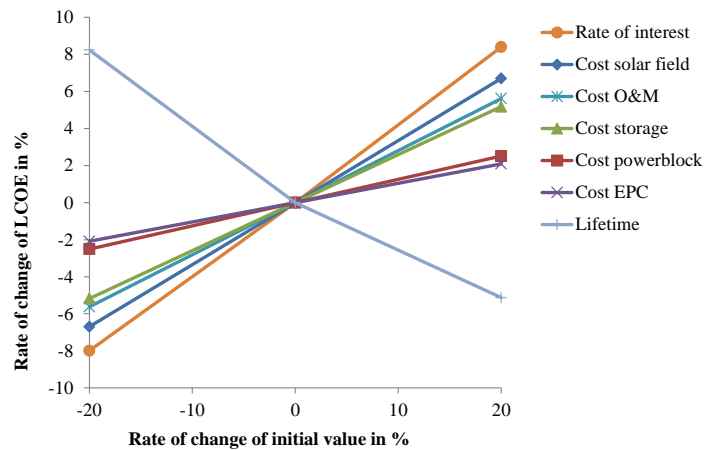
Figure 18. Sensitivity analysis of configuration b) with a three tank storage

2.4. Conclusion

A new concept for an active latent heat storage which uses a screw heat exchanger has been characterized experimentally with thermal oil and water/steam as heat transfer fluid. The overall heat transfer coefficients in the prototype during melting and crystallization have been determined. Based on calculated values of the convective heat transfer coefficients the overall heat transfer coefficients for a scaled-up SHE have been determined. For pressures as high as 100 bar, an alternative concept has been developed, which uses an organic fluid inside the flight of the SHE as working medium. Furthermore, a concept for a latent storage for DSG solar thermal power plants has been developed. With the generated measurement data of the test rig the simulation model could be validated. Three system configurations have been modelled and investigated: a DSG power plant with Fresnel collectors and a) a two tank storage, b) a three tank storage and for reference c) a system without storage. By varying parameters the minimal LCOE for each configuration have been determined. For a), the minimal LCOE are 0.143 €/kWh, for b) 0.134 €/kWh and for c) 0.129 €/kWh. This relates mostly to KPI 29, which aims at reducing the LCOE from the previous benchmark of 0.20-0.22 €/kWh. As storages can add to the market value of electricity, an increase in LCOE for the systems with storage is acceptable. A sensitivity study showed that the solar field costs have a high influence on the LCOE. By decreasing the storage cost by 20 %, the LCOE can be decreased by 5 %. In order to achieve this, the screw heat exchanger should be further optimized: The thermal efficiency of the screw heat exchanger should be increased and the temperature difference between the charging / discharging water and the PCM optimized.

This document is a brief summary of the activities of Fraunhofer ISE. For more detailed information refer to references [2, 3, 4 and 5], which are publicly accessible.

2.5. References

[1] Boye, J.-P. (2013): Strukturmechanische und wärmetechnische Optimierung eines Schneckenwärmeübertragers von einem Latentwärmespeicher für solarthermische Kraftwerke. Master thesis, Ansbach University of Applied Sciences, prepared at Fraunhofer Institute for Solar Energy Systems ISE

[2] Zipf, V.; Neuhäuser, A.; Rajpaul, V.; Richter, C. (2016): Combined solar heat and power system with a latent heat storage – system simulations for an economic assessment. In: AIP Conference Proceedings 1734 (1), S. 70033. DOI: 10.1063/1.4949180.

[3] Zipf, V.; Willert, D.; Neuhäuser, A.; Rajpaul, V.; Richter, C. (2016): Active latent heat storage with a screw heat exchanger – experimental results for heat transfer and concept for high pressure steam. In: AIP Conference Proceedings 1734 (1), S. 50044. DOI: 10.1063/1.4949142.

[4] Zipf, V. (2015): Schneckenwärmeübertrager in Latentwärmespeichersystemen. Tests und Wirtschaftlichkeitsstudie für solarthermische Anlagen. Aachen, Aachen: Shaker

[5] Zipf, V.; Neuhäuser, A.; Bachelier, C.; Leithner, R.; Platzer, W. (2015): Assessment of Different PCM Storage Configurations in a 50 MWel CSP Plant with Screw Heat Exchangers in a Combined Sensible and Latent Storage – Simulation Results. In: Energy Procedia. 69 , S. 1078-1088, DOI: 10.1016/j.egypro.2015.03.215.

[6] Schaumann, G. and K.W. Schmitz, Kraft-Wärme-Kopplung. 2010: Springer Verlag

3. CIEMAT Contribution

3.1. Use of liquid crystals as PCMs

The solution proposed by CIEMAT for the strategy of moving the storage medium is the use of thermotropic liquid crystals (LCs) as PCMs since they are materials that can absorb/release energy when they undergo a change between two liquid phases [1]. LCs are organic based materials whose molecules are usually formed by flat rigid cores containing one or more aromatic rings to which alkyl groups of a certain length are attached. This implies anisotropic molecules with rod-like, disk-like, banana or conical shapes with large dipolar moments and high polarizability, which leads to strong intermolecular interactions. Due to these interactions, liquid crystals present intermediate fluid phases between crystalline solid and isotropic liquid called mesophases. Figure 19 displays the energy-temperature curve for a generic rod-like liquid crystal where melting transition (solid crystal to mesophase) and clearing transition (mesophase to isotropic liquid) are indicated. From both of them, the transition of interest for thermal storage solution proposed by CIEMAT is the clearing process since it is the one taking place between two fluid phases. The movement of the PCM using LCs is intrinsically assured by its own nature of phase change between two fluid phases, with the additional advantages that energy exchange takes place by convection, sensible heat can be stored as well and that they can be used not only for heat storage but also for heat transport.
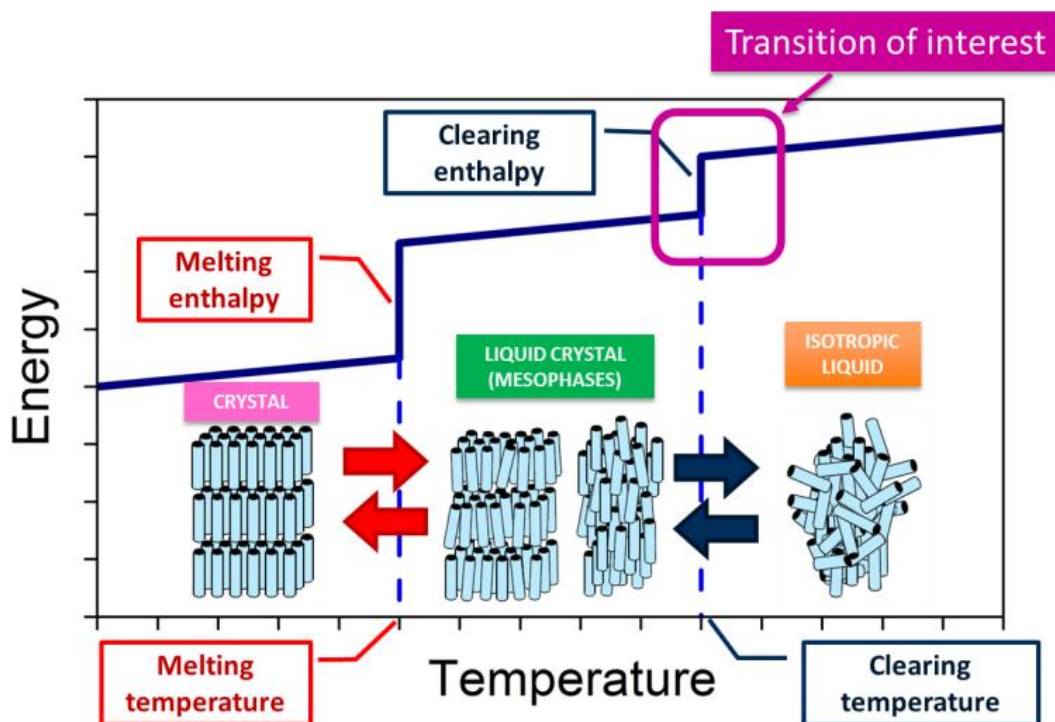

Figure 19. Energy curve as a function of temperature for a generic rod-like liquid crystal.

The main requirements of LCs for being used as PCMs are:

1. Clearing transition must be in the temperature range required by the DSG process.
2. Clearing enthalpy should be as high as possible in order to have a high storage capacity.
3. Low dynamic viscosity of all fluid phases to reduce pumping power.
4. Thermal stability upon long term operation so the storage properties are maintained during the life time of the storage system
5. From the implementation point of view: low environmental impact, low toxicity and low price

In order to find LCs with promising values of clearing enthalpies within the temperature range of DSG working conditions, the large review published by Acree and Chickos in 2006 [2] was thoroughly checked taking into account requirements 1 and 2. Figure 20 shows a dispersion of clearing temperature-enthalpy values corresponding to the selected LCs. As it can be seen, it is possible to find liquid crystals with clearing transitions in the temperature range of DSG applications (200ºC-300ºC) with enthalpies close to the most commonly considered PCMs like nitrate-based inorganic salts or eutectic mixtures (~100 kJ/kgK) [1].
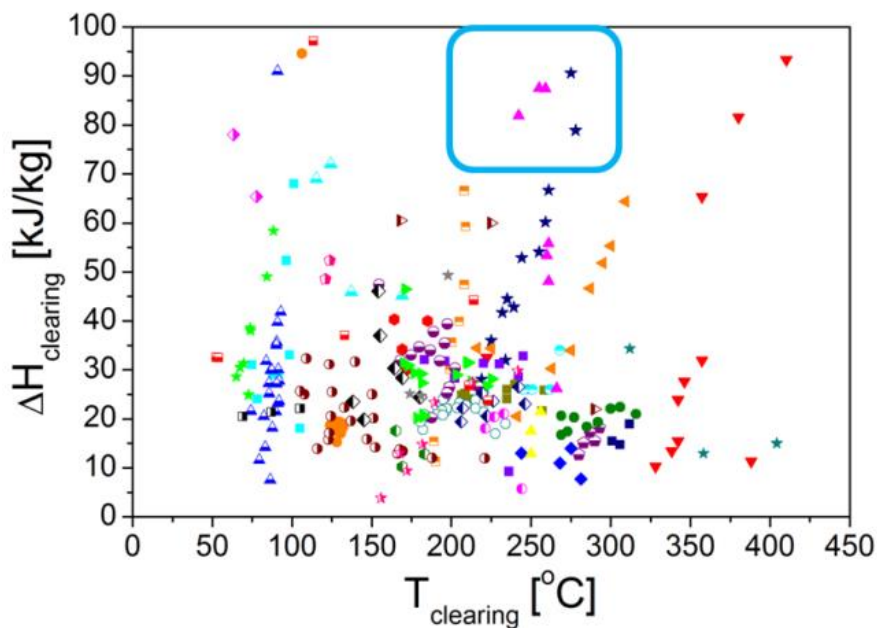
Figure 20. Clearing point enthalpy vs. clearing point temperature for various reported liquid crystals with thermal properties in the desired range for latent thermal storage [1].

The main advantage of using LCs as storage media is that they can exchange latent heat while keeping the ability to flow. This means that for the particular case of a CSP-DSG plant, the configuration could be very similar to a plant with a sensible liquid storage system. Figure 21 shows a scheme of a DSG plant with parabolic trough collectors in which a latent heat thermal storage system based on a LCs has been implemented with a two-tank system configuration. With this configuration the hot tank contains the isotropic liquid phase and the cold tank contains the liquid crystal phase. In the same way, a single tank thermocline system could be figured out.
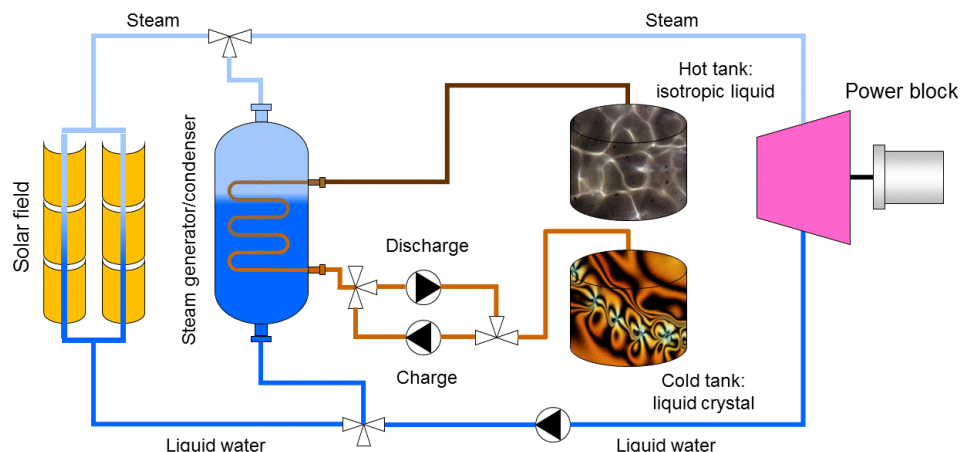
Figure 21: Potential scheme of a solar DSG plant with a latent storage system using LCs as PCMs.

As a starting point, one of the LC families included in Figure 20, [2], was selected for proving the viability of LCs latent storage materials. This family corresponds to the N,N-dialkanoyl-2,3,5,6-tetramethylbenzene-1,4-diamines with alkyl chains of different lengths, [3]. In Figure 22 the molecular structure of this LC family (left) and the reported values for transition temperatures and clearing enthalpy as a function of alkyl length (right) are displayed. Derivatives with alkyl chains of n=6-9 carbon atoms display clearing temperatures (top of the column) around 300ºC and clearing enthalpies above 50 kJ/kg. Therefore derivatives with n=7 and n=9 were synthetized and their thermal properties where obtained by differential scanning calorimetry (DSC). Both derivatives showed the expected values of thermal properties however, a strong degradation was observed immediately upon clearing, which indicates that this family is not suitable for thermal storage applications.
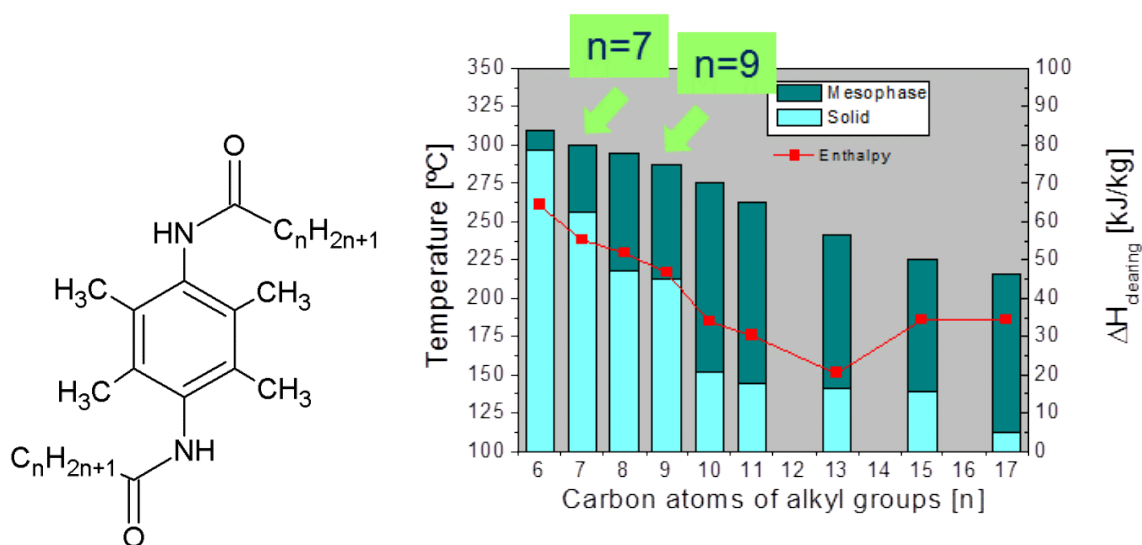
Figure 22. Molecular structure of N,N-dialkanoyl-2,3,5,6-tetramethylbenzene-1,4-diamines and variation of phase transition temperatures and clearing enthalpy with the alkyl chain for derivatives from n=6 to n=17.

In general, liquid crystal experts agree that LCs with strong intermolecular interactions affecting the clearing process should be the most suitable for this thermal storage application. These strong interactions are expected to occur in compounds with various aromatic rings and with functional groups that can form intermolecular H-bonds in the mesophase. Actually, the reason why the LC family of Figure 22 displays clearing transitions at high temperatures with quite high enthalpy values must be related to the formation of intermolecular H-bonds between amine and carbonyl groups. In order to check other compounds with strong intermolecular interactions but with better thermal stability, the LC family of 4'-n-alkoxybiphenyl-4-carboxylic acids (n-BPhCOOH) was considered. These compounds not only have two aromatic rings in the molecule but also the acidic groups are able to form intermolecular H-bonds leading to dimeric species in the mesophase. Moreover their preparation is already reported in the literature as well as their phase transition temperatures and the kind of mesophase observed by polarized-light microscopy [4]. The general molecular structure together with the mesogenic behavior in terms of transition temperatures for each derivative of this family are displayed in Figure 23.
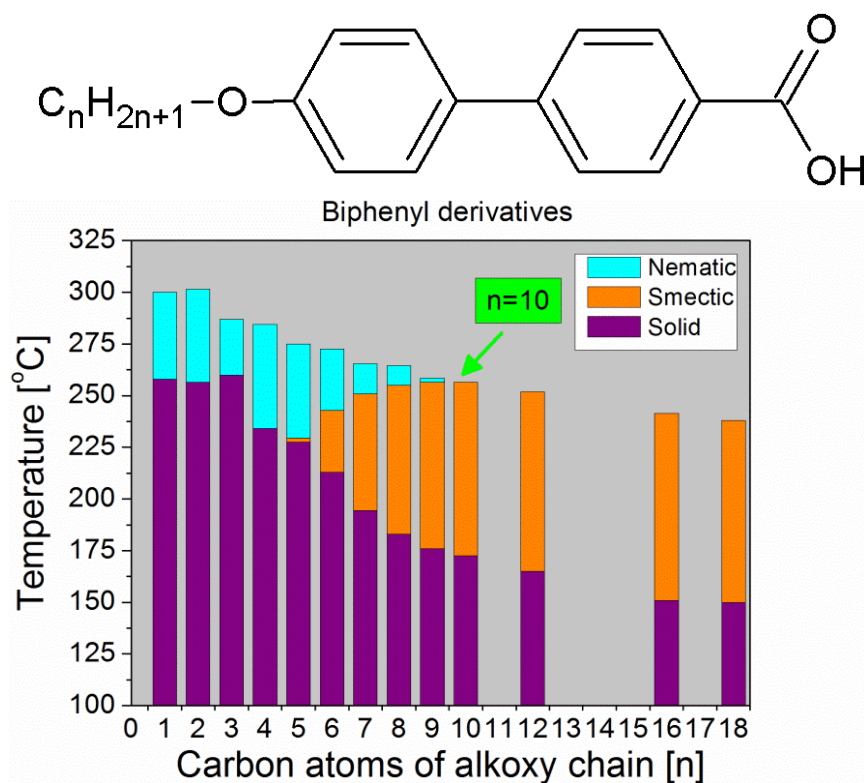
Figure 23. Molecular structure of 4'-n-alkoxybiphenyl-4-carboxylic acids and variation of phase transition temperatures with the alkoxy chain for derivatives from n=1 to n=18.

This figure shows that all derivatives present clearing temperatures (top of the column) varying from nearly 300 °C to 240 °C as alkoxy chain increases from n = 1 to n = 18. Therefore, in order to prove the feasibility of these LCs as PCMs the derivative with n=10 carbon atoms in the alkoxylic chain (10-BPhCOOH) was chosen for preparation. Other important reasons for choosing one derivative of this family are the commercial availability of

precursors and the simple synthetic route [4]. This compound was characterized by polarized-light microscopy for checking its liquid crystal behavior together with differential scanning calorimetry (DSC), thermogravimetric (TG) and thermal cycles in a PDI controlled oven for obtaining the thermal properties and studding its thermal stability under thermal cycling. Additional properties like specific heat capacity (C_p) and dynamic viscosity were measured as well.

Figure 24 (left) displays the scans of the first and second heating/cooling DSC cycles of 10-BPhCOOH, where we can see that it has a crystal/mesophase transition at around 170 ºC with 35 kJ/kg melting enthalpy and a mesophase/isotropic liquid transition at 251 ºC with 55 kJ/kg clearing enthalpy. It is interesting to note that this compound shows a wide mesophase range (80 ºC), which would largely prevent its freezing in case of an eventual temperature decrease due to undesired thermal losses.

In relation to the transition energies, it is worth remarking that the clearing enthalpy is much higher than melting enthalpy (55 kJ/kg vs. 35 kJ/kg), which confirms that intermolecular forces in the mesophase are fairly strong as expected from the involvement of H-bonds and the two aromatic rings.
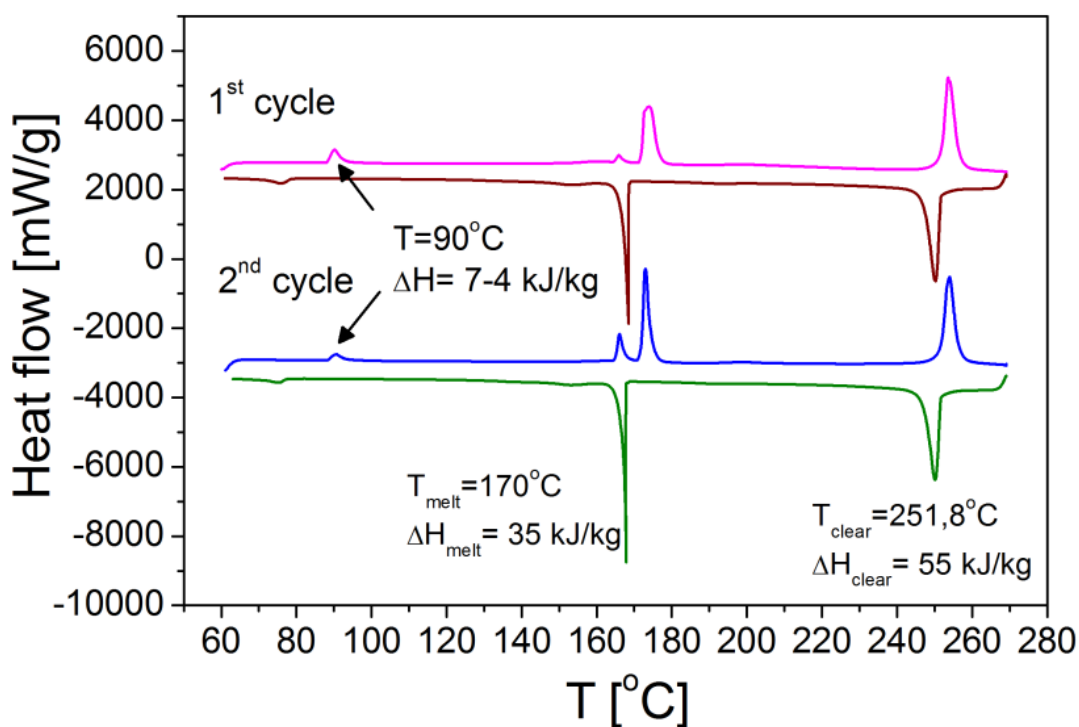
Figure 24. Differential scanning calorimetry (DSC) curves of first and second heating/cooling cycle for 10-BPhCOOH.

The results of DSC analysis together with the values of viscosity and C_p of the mesophase are recorded in Table 3. All values indicate that in principle this liquid crystal fulfills quite well the requirements for being used as latent storage medium for DSG applications.

Table 3. Thermo-physical parameters measured for 10-BPhCOOH.

Derivative n=10	
$T_{clearing}$	251 ºC
$\Delta H_{clearing}$	55 kJ/kg
Viscosity	0.18-0.6 Pas
C_p mesophase	2.4 kJ/kgK

For studying the thermal stability of 10-BPhCOOH, 11 consecutive thermal cycles around the clearing temperature were performed in a DSC apparatus. It was observed that clearing temperature remained constant during the cycling for both heating and cooling processes. However, clearing enthalpies tended to decrease with cycling from about 55 kJ/kg in the first cycle to around 50 kJ/kg after 11 cycles. Hence it seems that some degradation takes place in 10-BPhCOOH upon cycling.

Thermal behavior of 10-BPhCOOH was also studied by means of thermogravimetric (TG) analysis by heating a sample up to 550ºC under Ar and monitoring its mass variation during the process. The corresponding differential (dTG) showed that two main degradation processes take place (at 386 ºC and 435 ºC) and that only 1% mass was lost at 290 ºC, which would indicate that 10-BPhCOOH is expected to be stable under Ar at least up to 40 ºC above its clearing temperature (251 ºC). However, the decrease of clearing enthalpy observed upon preliminary cycling in DSC experiments performed under N_2 [5] prove that TG results must be taken with care and that further stability experiments need to be carried out.

Therefore, in order to assess the thermal stability under conditions as close as possible to real working conditions, a 10-BPhCOOH sample of about 1 g was kept in a PID controlled oven under air and cycled between 240ºC and 255ºC with stand-by times at each temperature of 2 hours. Sample temperature was monitored during the whole experiment with the help of an external thermocouple. In Figure 25 (left) temperature-time curves of the melting process for 2nd to 4th cycles are displayed. Only in the curve of the 2nd cycle a shoulder around clearing temperature can be slightly distinguished, whereas already in the 3rd cycle a straight segment is obtained. The picture of Figure 25 (right) shows the sample appearance after 16 thermal cycles. The 10-BPhCOOH sample that was initially white has become completely black, which clearly indicates that it has undergone strong degradation. Unfortunately the thermal decomposition inferred from DSC cycles is clearly confirmed by oven cycles. This decomposition after clearing transition is due to the high reactivity of acidic group, which is probably promoted by the high temperature range in which clearing process takes place.
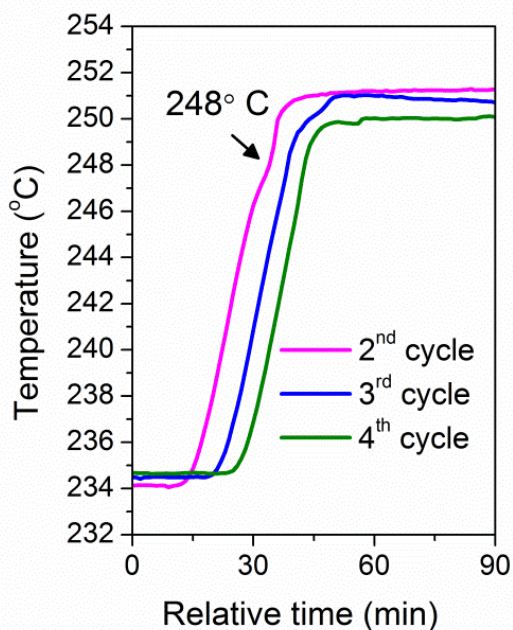
Figure 25. Temperature/time curves of thermal cycles performed around clearing temperature (i. e. between 240ºC and 255ºC) (left). 10-BPhCOOH sample appearance after 16 thermal cycles (right).

In parallel to this work, a preliminary estimation of the figures of merit of potential LC candidates, in terms of phase change enthalpies and specific cost, was performed [6]. The results for an LC-based two tank configuration were compared with latent storage systems containing low conductivity inorganic salts with embedded heat transfer enhancement structures, which is the option widely considered today for overcoming the PCM conductivity issue. This study showed that LCs with a phase change enthalpies similar to the displayed by inorganic PCMs could be competitive with the latter in terms of costs. Actually, the higher the plant size or the longer storage time, the higher the LC price that could be afforded. However, independently on the costs, it should be highlighted that the main advantage of using LCs as PCMs for a latent storage subsystem in a DSG plant is its capability of providing constant discharge power, unlike the inorganic PCMs. This advantage should undoubtedly have economic consequences, since it will improve both the annual yield of the plant and its dispatchability.

3.2. Conclusion

CIEMAT is exploring the feasibility of the innovative approach of using liquid crystals (LCs) as moving phase change materials (PCMs) in latent heat storage systems in DSG applications. The requirements that LCs have to fulfil for such application have been established and a tentative configuration of a DSG-CSP plant with a LC-based two tank storage system has been presented. In order to prove the feasibility of this approach several compounds have

been prepared and tested. The last one, an alkoxy-derivative of biphenylbenzoic acid, was expected to display high values of transition temperature and enthalpy due to strong intermolecular interactions related with H-bonds. Although preliminary results in terms of thermo-physical properties were very promising, thermal stability tests proved that this compound undergoes strong degradation under the expected working conditions. One of the problems faced in this research is that, in most of the times, the information found in the literature on LCs thermo-physical behaviour is limited to their mesogenic phase, being pretty scarce or inexistent the information on the stability of the isotropic liquid phase –see Figure 22 and Figure 23-. Thus, it is necessary to check such stability for the prepared compounds. In any case, since the organic nature of LCs allows tailoring their thermal properties, it should be possible to prepare other compounds that fit the requirements for DSG thermal storage applications keeping an eye on their thermal stability. In this way we believe that this totally new perspective of LC application is worth being developed in order to demonstrate the experimental feasibility of the concept.

This document is a brief resume of the current activities of CIEMAT. For more detailed information you can refer to the open access papers [6, 7].

3.3. References

[1] R. Bayón, E. Rojas. Liquid crystals: a new approach for latent heat storage. International Journal of Energy Research 37 (**2013**) 1737-1742. doi: 10.1002/er.3121.

[2] Acree W. E., Chickos J. S.: Phase change enthalpies and entropies of liquid crystals. Journal of Physical and Chemical Reference Data 35 (**2006**) 1051-1330.

[3] H. Hosokai, K. Iuchi, T. Tumagai, Y. Matsunaga. Mesomorphic behaviour of N,N-dialkanoyl-2,3,5-trimethylbenzene1,4-diamines and 2,3,5,6-tetramethylbenzene-1,4-diamines. Liquid Crystals 26 (**1999**) 699-703. doi: 10.1080/026782999204769.

[4] G. W. Gray, J. B. Hartley, B. Jones. Mesomorphism and chemical constitution. Part V. The mesomorphic properties of the 4'-n-alkoxydiphenyl-4-carboxilic acids and their simple alkyl esters. J. Chem. Soc. (1955) 1412-1420.

[5] R. Bayón, S. Coco, M. Barcenilla, P. Espinet, G. Imbuluzqueta, J. Hidalgo, E. Rojas. Storing latent heat with liquid crystals. Is it a feasible option? European Conference on Liquid Crystals 2015, Manchester (UK), September 2015 (Poster).

[6] E. Rojas, R. Bayón, E. Zarza. Liquid crystals: a different approach for storing latent energy in a DSG plant. International Conference on Concentrating Solar Power and Chemical Energy Systems, SolarPACES **2014**, Beijing, September 2014. (Oral presentation). Proceedings in Energy Procedia 69 (**2015**) 1014-1022. doi:10.1016/j.egypro.2015.03.197.

[7] R. Bayón, S. Coco, M. Barcenilla, P. Espinet, G. Imbuluzqueta, J. Hidalgo, E. Rojas. Feasibility of Storing Latent Heat with Liquid Crystals. Proof of Concept at Lab Scale. Applied Sciences 6 (**2016**) 121-131. doi:10.3390/app6050121.